RSC Advances

ROYAL SOCIETY OF CHEMISTRY

www.rsc.org/advances

Block – shaped Pure and doped $Li_4Ti_5O_{12}$ containing a high content Li_2TiO_3 dual phase: Anode with excellent cycle life for the high rate performance of lithium-ion batteries

Emad M. Masoud[a,*], Sylvio Indris[b]

[a]Chemistry department, Faculty of science, Benha University, 13518 Benha, Egypt

[b]Karlsruhe Institute of Technology, Institute for Applied Materials (IAM), Hermann-von-Helmholtz-Platz 1, D-76344 Eggenstein-Leopoldshafen, Germany

Abstract

Pure and doped lithium titanate samples ($Li_4Ti_5O_{12}$, $Li_4Ti_{4.9}x_{0.1}O_{12}$, x = Ni^{2+}, Cu^{2+} and Zn^{2+}) are prepared using simple solid state reaction. All lithium titanate samples are characterized using X-ray diffraction, Fourier transmission infra – red spectra and scanning electron microscopy. X-ray diffraction patterns show the cubic spinel structure of $Li_4Ti_5O_{12}$ with a presence of different content of Li_2TiO_3 crystalline second phase, high for the doped samples and low for the pure one. Fourier transmission infra – red spectra also confirm the spinel structure. Scanning electron microscopy shows block-shaped particles with different particle size distribution. The pure lithium titanates composite sample shows more efficient electrochemical performance than the doped ones at the high discharge rates (2-30C) and the opposite is observed at the low ones (0.1,0.5C). The efficiency and cycle life of the pure lithium titanates composite at high rate (30C) are higher and better than that of low one (0.1C), making the pure one as a promising anode material for the high rate lithium – ion batteries. All results are collected and discussed.

Keywords: Anode material; electrochemical measurements; electrical properties; energy storage; Lithium –ion batteries

* Corresponding author: emad.youssef@fsc.bu.edu.eg ; emad_masoud1981@yahoo.com ; Tel: 00201203532343

1. Introduction

Stimulated by the urgency of environmental protection and the exhaustion of fossil fuel reserves, more and more attention have been paid to the development of lithium ion batteries with high power density for the applications of large format energy storage system, such as electric vehicles (EVs) or hybrid electrical vehicles (HEVs) [1]. At present, one of the main factors that hinders the commercialization of EVs/HEVs is the low rate performance of batteries. Therefore, an urgent step for the significant market penetration of EVs/HEVs is the development of a high rate battery system. Anode is one of the most important parts of a battery. Considering carbon based anodes, the low operating potential of 100 mV (vs. Li^+/Li) tends to induce the growth of lithium dendrites at high charge/discharge rates, which will make a short circuit possible [2]. Alternative anode materials of silicon and tin have been extensively studied for their attractive specific capacities [3]. However, the poor cycle stability caused by immense volume expansion in the process of lithiation stands in the way of commercialization. In spite of less competitive specific energy density relative to carbon, tin, and silicon-based materials, spinel lithium titanate ($Li_4Ti_5O_{12}$) is considered as one of the most promising anodes for its higher discharge/charge plateau (about1.55 V vs. Li^+/Li) and zero strain characteristic which can provide possible solutions to the challenges of safety and cycle stability for advanced batteries [4-6]. Evidently, it is the

poor rate performance resulted from quite low electronic conductivity ($<10^{-13}$S cm^{-1}) [7] and intermediate Li ion conductivity of pristine $Li_4Ti_5O_{12}$ that retards it from commercialization.

Traditional methods for improving electronic conductivity and ionic conductivity mainly focus on cation doping (Mg, Al, V, etc. [7-11]), surface modification (carbon, polyacene, etc. [12-17], and size control [18,19]. More recently, composites of $Li_4Ti_5O_{12}$/Ag [20-23], $Li_4Ti_5O_{12}$/Au [24], $Li_4Ti_5O_{12}$/Cu [25,26], and $Li_4Ti_5O_{12}$/CNT[27] have been widely investigated to improve particle-to-particle and particle-to-current collector electric contact. Alternatively, nano composites of $Li_4Ti_5O_{12}$ and metal oxides can provide rich grain boundaries with high concentration of diffusion-mediating defects, which make fast diffusivity possible. In this regarding, dual-phase $Li_4Ti_5O_{12}$-TiO_2 has been synthesized with improved rate capability [28-30]. According to the literature review, there is one report considering the compact of Li_2TiO_3 second phase traces on the electrochemical performance of $Li_4Ti_5O_{12}$ [31]. Here, we want to study the effect of doping by Zn^{2+}, Cu^{2+} and Ni^{2+} on the electrochemical performance of $Li_4Ti_5O_{12}$ in presence of a high content crystalline second phase of Li_2TiO_3 at low and high rates with comparing to the pure one, to show which can deliver a high capacity and good cycle life at high rates.

2. Experimental

2.1 Preparation of samples

All samples were prepared using solid-state reaction method. Li_2CO_3 (Merck, 99.99%), TiO_2 (Sigma-Aldrich, 99.9%), NiO (Sigma-Aldrich, 99.99%), CuO (Sigma-Aldrich, 99.99%) and ZnO (Sigma-Aldrich, 99.99%) powders were used to prepare the pure and doped lithium titanate samples ($Li_4Ti_5O_{12}$, $Li_4Ti_{4.9}x_{0.1}O_{12}$, x = Ni^{2+}, Cu^{2+} and Zn^{2+}). 4:5 molar ratio of Li_2CO_3 : TiO_2 for the pure sample and 4:4.9:0.1 molar ratio of Li_2CO_3 : TiO_2 : dopant source for the doped samples were firstly ball-milled in presence of ethanol as a dispersion medium for 3 hrs. in a ball-milling machine to homogenously mix the powders. In all cases, 3 mol % excessive Li_2CO_3 was added to compensate for Li_2O evaporation during the synthesis at high temperature. All samples were dried at 90˚C for 30 minutes to remove the ethanol, and then the milled mixtures were calcined at 800˚C for 4 hrs. in air.

2.2 Characterization of samples

X-ray diffraction analysis was performed on STOE STADI P diffractometer (Cu-Kα radiation, Germanium monochromator, Debye-Scherer geometry). The samples were measured at room temperature in the range from $2\theta = 10^o$ to 70^o. The XRD phases present in the samples were identified with the help of ASTM Powder Data Files. The infrared

spectra of samples were recorded in the range of 400 – 4000 cm^{-1} using a Brucker-FTIR. The morphology of samples were examined using scanning electron microscopy (SEM, JEOL JSM – 6700F) operated at an accelerating voltage of 5 KV.

The electrical measurements were carried out in the form of pellet. The two parallel surfaces of the pellet were coated with silver paste to ensure good electrical contact. The sample was located in a sample holder inside a cryostat with a temperature controller of ± 0.01°C accuracy. The electrical conductivity was measured at a constant voltage (1 volt) using a programmable automatic LCR bridge (Model RM 6306 Phillips bridge).

2.3 Electrochemical measurements

For setting up the experimental cell, pure and doped samples (active material), (80 wt.%) , was mixed with carbon black (10 wt.%) and PVDF (10 wt.%) in presence of n- methylpyrrolidinone to make the mixture homogeneous and then the mixture was left on a stirrer for 2 hrs. to get the homogeneity material (Slurry). Then, the mixed slurry was deposited on a thin copper foil by a doctor blade process and dried at 80 ˚C for 2 hrs. afterward. The covered copper foil was finally punched into round pieces with a diameter of 12 mm. The as prepared electrodes were stored in a vacuum oven for further drying of another 12 hrs. before they were transferred into a glove box for battery assembly. The glove box was circulated with argon gas (99.99%) to ensure a clear atmosphere (O_2 < 5

ppm, H_2O < 5 ppm). The counter electrode used in the half cell was lithium foil. 1 M $LiPF_6$ in ethylene carbonate (EC)-diethyl carbonate (DEC) (1:1 in volume) was chosen as the electrolyte. A glass fiber separator (whatman GF/C) was used for separating the cathode and a lithium metal anode. The cells were galvanostatically charged and discharged using an Arbin battery cycler (BT2000, Arbin instruments) in the scan rate of 1 mVs^{-1} to perform charge – discharge processes for the assembled battery. The charge –discharge processes were performed at a voltage between 0 and 3 V at different low (0.1,0.5C) and high (2-30C) rates.

3. Results and discussions

XRD spectra of all pure and doped samples are shown in Fig.1A. The figure peaks showed the cubic spinel structure of the samples ($Li_4Ti_5O_{12}$) [JCPDS 26-1198] with some other intensive peaks characteristic to a crystalline second phase. The other crystalline peaks were identified as monoclinic Li_2TiO_3 phase [JCPDS 33-0831]. The sharp crystalline peaks of each $Li_4Ti_5O_{12}$ and Li_2TiO_3 indicate a good crystalline structure with no impurity phases demonstrating that Ni^{2+}, Cu^{2+} and Zn^{2+} ions have been successfully introduced into the lattice structure of $Li_4Ti_5O_{12}$. Another important remark can be observed by the figure, is that the intensity of Li_2TiO_3 peaks increases with the doping effect of Ni^{2+}, Cu^{2+} and Zn^{2+} ions. This shows that the doped samples have a high content crystalline

second phase of Li_2TiO_3 compared to the pure one. To further confirm the doping process, quantitative x-ray analysis was performed by a definite peak of each phase. Firstly, the peak characteristic to $Li_4Ti_5O_{12}$ phase, **(111),** was partially enlarged, Fig1B. As we can see by a close inspection, there is a small shift to lower degrees for the doped samples compared to the pure one, confirming that Ni^{2+}, Cu^{2+} and Zn^{2+} ions having larger ionic radii (0.69Å, 0.73Å and 0.74Å for Ni^{2+}, Cu^{2+} and Zn^{2+} ions, respectively) than that of Ti^{4+} (0.60 Å) have been successfully doped into the host crystal structure of $Li_4Ti_5O_{12}$. Also, lattice parameter and unit cell volume values increasing of doped samples compared to the pure one confirmed the successful doping process, Table 1. Secondly, the peak characteristic to Li_2TiO_3 phase**,(020),** was also partially enlarged, Fig.1C. The figure showed a small shift to larger degrees for the doped samples compared to the pure one, and to be more sure that this shift was caused by the crystalline second phase presence and not by the doping of any ion, unit cell volume was calculated, Table 2, to show a stable value for all samples before and after doping. This shows that we have a good doping process into the cubic $Li_4Ti_5O_{12}$ spinel structure not into the monoclinic Li_2TiO_3 structure. The weight ratio of Li_2TiO_3 of all samples was **estimated** using the relative peak intensity, Table 2. The table showed a high weight ratio of Li_2TiO_3 in all investigated samples, and a high content in the doped samples compared to the pure one.

The FT-IR spectra of pure and doped lithium titanates composites samples calcined at 800 ˚C are given in Fig. 2. It can be clearly observed that there are two absorption bands located at 643 and 449 cm^{-1}. These two absorption bands indicate the symmetric and asymmetric stretching vibrations of the octahedral [TiO_6] groups respectively [32], confirming the existence of the normal spinel structure. This is in agreement with the XRD results shown in Fig. 1. The band at 1625 cm^{-1} is attributed to H-O-H bending vibration [33]. The band at 3470cm^{-1} is attributed to the stretching vibrations of the hydrogen-bonded OH groups.

The absence of other bands characteristic to other metal oxides also confirms the formation of lithium titanates composites and demonstrates that all doped ions have been introduced into the lattice structure, as confirmed by XRD.

All the SEM images of lithium titanates composites samples calcined at 800˚C for 4hrs. are similar, so we set the pure lithium titanates composite sample as an example to observe the morphology of the investigated sample, Fig.3. It can be seen clearly that the sample exhibits block-shaped particles with different particle size distribution. The particle size, with a wide distribution from less than 100 nm to more than 1000 nm, has a medium value of approximately 500 nm.

To show the performance of the pure and doped lithium titanates composites as anode in lithium batteries, different charge – discharge

processes were performed at a high rate range of 2-30C (2,5,10,20,30C) and a potential range of 0-3V , Fig. 4.

The figure showed that all pure and doped lithium titanates composites have good initial discharge capacity and cycling stability at all the high rate range (2-30C). In general, the pure lithium titanates composite showed the highest delivering one of discharge capacity compared to the other ones, especially at rates of 2 and 10 C. At the same time, the Zn^{2+} - doped lithium titanates composite was the lowest delivering one of discharge capacity in the time that the other doped composites (Cu^{2+}, Ni^{2+}) did not show a clear comparison behavior of discharge capacity delivering, the Cu^{2+} - doped sample has the highest discharge capacity value compared to the Ni^{2+} - doped one at only rates of 5,10,20 and 30C. The only case that Ni^{2+} - doped sample is higher than that of Cu^{2+} was observed at the rate of 2C. As the discharge rate increased, the capacities gradually decreased. More notably, at all rates of cycling performance and for all pure and doped lithium titanates composites, after the first cycle, the capacity retention begins to be more stable.

To investigate the effect of doping at low (0.1, 0.5C) and high rates (10,20,30C), the values of initial discharge capacity of all investigated samples were determined , Table 3. It is obvious from the table that the Cu^{2+} - doped lithium titanates composite has the highest discharge capacity (319, 172 mAh/g) at the low rates (0.1, 0.5C), but at the high

rates (10,20,30C), the pure sample has the highest values (123, 95, 91 mAh/g). Also, the table shows the values of lithium ion diffusion (D) calculated using the following equation, $D = R^2T^2/2A^2F^4\sigma^2_wC^2$ (1)

where σ_w, the Warburg impedance coefficient, w, the angular frequency, R, the gas constant, T, the absolute temperature, A, the surface area, F, the Faraday's constant, and C, the molar concentration of Li ions.

The table showed that the pure lithium titanates composite has the highest lithium ion diffusion value, 5.55 $x10^{-13}$ cm^2/s, compared to the other doped ones. At the same time, this value is higher than that of the pristine $Li_4Ti_5O_{12}$ [34], the enhancement caused by the low content of Li_2TiO_3 crystalline second phase.

From all the above results, we can conclude that our lithium titanates composites samples electrochemical performance can be divided into two parts, the pure composite is the best at the high rates (2-30C), and Cu^{2+} - doped composite is the best at the low rates (0.1,0.5C). This can be attributed to two different factors competing at the same time, doping and the different content of crystalline second phase, Li_2TiO_3. The high crystalline second phase content of doped lithium titanates composites compared to the pure one at the high rates (2-30C) reduced the lithium ion diffusion (Table 3) , and as a result, the discharge capacity reduced, showing the pure sample is the best (The crystalline content of Li_2TiO_3 is the negative predominant factor). On the other hand, at the low rates

(0.1,0.5C), the doped samples showed the doping factor as of the positive predominant, and the Cu^{2+} - doped is the best. The high initial discharge capacity of Cu^{2+} - doped composite sample compared to Ni^{2+} and Zn^{2+} ones may be attributed to the suitable unit cell volume in presence of the high content of Li_2TiO_3.

For the cycle life and capacity retention, all pure and doped composites showed excellent cyclability at the high rate (30C) compared to previous similar systems as will be shown hereafter, and this behavior can be attributed to the structure stability against crystal breakdown performed in presence of the crystalline second phase, Li_2TiO_3. Also, presumably, the good electrochemical performance of dual-phase $Li_4Ti_5O_{12}$–Li_2TiO_3 could be attributed to the $Li_4Ti_5O_{12}$–Li_2TiO_3 featuring abundant phase interfaces, which can possess an interfacial storage mechanism [35-37]. Namely, the lithium-ions and electrons are stored separately at the interfacial region between two neighboring phases to generate the capacitance, favoring for the high rate capability [35-37].

To show the difference between the performance of pure lithium titanates composite at low (0.1C) and high (30C) rates, the discharge capacity against cycle number (the first 10 cycles) was investigated and shown in fig. 5. The figure shows that the pure lithium titanates composite at low rate delivered high initial discharge capacity,160 mAh/g, and then a sharp decrease was observed up to 90 $mAhg^{-1}$ to end

the 10^{th} cycle life with a capacity of 73 $mAhg^{-1}$. On the other hand, the pure lithium titanates composite at high rate showed an initial discharge capacity of 91 $mAhg^{-1}$ to end the 10^{th} cycle with a capacity of 70 $mAhg^{-1}$. This shows that the pure composite at 30 C has a better discharge capacity value and cycle life than that at 0.1C. Also, the columbic efficiency was calculated for the same two samples, Fig 6. It is clearly shown that the 30C - pure lithium titanates composite has higher efficiency (~100% for the last cycle) than the 0.1C one (~80% for the last cycle).

Fig. 7 (A,B) shows the galvanostatic lithium insertion/extraction curves for the 10^{th} cycle of pure lithium titanates composite at low (0.1C) and high (30C) rates between 0-3V. Fig. 7B showed that the composite has two obvious almost straight regions of reduction and oxidation at about 1.5V and 1.68V, respectively, and which are assigned to the insertion and extraction of Li^+ ions [31]. Besides the reduction –oxidation, capacitive plateaus at lower potential are also found during the scan, demonstrating that both of faradic reaction and double layer capacitance are involved in the electrochemical process [31].In Fig. 7A, the two straight regions are not appeared and the two reactions of insertion and extraction of Li^+ ions appeared as first two plateaus at a range of 3-1V and 1-0.5V, respectively, and then the other two ones demonstrates both of faradic reaction and double layer capacitance like that of Fig 7B. Here we can

conclude that the pure composite at 30C has a better nature of insertion/extraction reactions than that of 0.1C.

To show the efficiency of our pure lithium titanates composite as an anode for the high rate performance in lithium ion batteries , our sample was compared to the previous reported performances of pure [38-40] and composite of $Li_4Ti_5O_{12}$ [31] at high rates, Table 4.

To further study the properties of the pure lithium titanates composite as a good anode material for the high rate performance of lithium ion batteries, the AC-electrical properties (ionic conductivity and complex impedance) were also investigated at room temperature (295K) and different frequencies, Fig.8 (A,B).

Fig.8 A shows the variation of 1og σ_{AC} against log F. It can be seen that the conductivity increases with frequency increasing. This can be attributed to the ability of lithium cation to rotate rapidly in directions matching with the directions of the applied current, demonstrating the high value of lithium ion diffusion, Table 3. Also, the ionic conductivity at F = 1MHz of the pure composite was determined to equal 2.02 x 10^{-7} $ohm^{-1}.cm^{-1}$.

The spectrum of complex impedance, Fig.8B, showed a straight line at room temperature. This can be attributed to the blocking electrode that results in a charge polarization in the bulk of the composite [41], and as a result, the electrical double layer at each interface will lead to increase the

impedance against ion motion with decreasing frequency. The bulk ionic conductivity was determined to equal $2.24x10^{-5}$ $ohm^{-1}.cm^{-1}$ at F = 1MHz. The equivalent circuit was also determined and shown in Fig.8 B. Where R_1 is the bulk resistance, C_1 is the bulk capacity and C_2 is a capacity of bulk electrode – electrolyte interface. The values of dielectric constant (ε`) and dielectric loss (ε``) were calculated to equal 391 and 7516, respectively. All values of ionic conductivity, bulk ionic conductivity, dielectric constant and loss showed that li-ions have a good diffusion and orientation within the crystalline network structure of the titanates composite, making it a promising anode for the high rate lithium ion batteries.

Conclusions

Pure and doped lithium titanate samples containing a high crystalline second phase content of Li_2TiO_3 ($Li_4Ti_5O_{12}$/ Li_2TiO_3, $Li_4Ti_{4.9}x_{0.1}O_{12}$ / Li_2TiO_3, x = Ni^{2+}, Cu^{2+} and Zn^{2+}) were prepared using simple solid state reaction. All lithium titanates composites samples were characterized using XRD, FT-IR and SEM. XRD patterns showed the cubic spinel structure with a presence of different content of Li_2TiO_3 crystalline second phase. The doped samples showed higher content of the crystalline second phase than that of the pure one. The pure lithium titanates composite showed more efficient electrochemical performance than that of the doped ones at the high discharge rates (2-30C). On the

other hand, the doped lithium titanates composites showed more efficient electrochemical performance than that of the pure one at the low rates (0.1, 0.5C), and the Cu^{2+} - doped composite was the best. The efficiency and cycle stability of the pure lithium titanates composite at high rate were higher than that of low rate. The pure composite delivered a high initial discharge capacity of 91 $mAhg^{-1}$ at 30C with room temperature lithium ion diffusion equals 5.55 x 10^{-13} cm^2/s. After 50 cycle, the pure composite delivered a discharge capacity of 65 $mAhg^{-1}$ at 30C, showing an excellent cycle life. The ionic conductivity, bulk ionic conductivity, dielectric constant and dielectric loss of the pure composite at room temperature and 1MHz frequency were determined to equal 2.02 x 10^{-7} $ohm^{-1}.cm^{-1}$, 2.24x10^{-5} $ohm^{-1}.cm^{-1}$, 391, 7516, respectively. The electrochemical performance of the pure composite shows a good discharge capacity with excellent cycle life at 30C, making it a promising anode material for the high rate lithium – ion batteries.

Acknowledgments

I, Dr. Emad M. Masoud, would like to extend my sincere thanks to Prof. Dr. Juergen Meyer (Tuebingen University, Germany) for his support and helping me to perform my research activity plan through my research stay period at Germany (DAAD scholarship) (GERSS, German Egyptian Research Short-term Scholarship).

References

[1] M. Armand, J.M. Tarascon, Nature 451 (2008) 652-657.

[2] F. Orsini, A. Du Pasquier, B. Beaudouin, J. Tarascon, M. Trentin, N. Langenhuizen, E. De Beer, P. Notten, J. Power Sources 81 (1999) 918-921.

[3] J.W. Li, A.J. Zhou, X.Q. Liu, J.Z. Li, J. Inorg. Mater. 28 (2013) 1207-1212.

[4] T. Ohzuku, A. Ueda, N. Yamamoto, J. Electrochem. Soc. 142 (1995) 1431-1435.

[5] K. Zaghib, M. Simoneau, M. Armand, M. Gauthier, J. Power Sources 81 (1999)300-305.

[6] A. Guerfi, S. Sevigny, M. Lagace, P. Hovington, K. Kinoshita, K. Zaghib, J. Power Sources 119 (2003) 88-94.

[7] C. Chen, J. Vaughey, A. Jansen, D. Dees, A. Kahaian, T. Goacher, M. Thackeray, J. Electrochem. Soc. 148 (2001) A102 A104.

[8] T.F. Yi, Y. Xie, J. Shu, Z. Wang, C.B. Yue, R.S. Zhu, H.B. Qiao, J. Electrochem. Soc.158 (2011) A266-A274.

[9] Y.-R. Jhan, C.-Y. Lin, J.-G. Duh, Mater. Lett. 65 (2011) 2502-2505.

[10] Z. Wang, G. Chen, J. Xu, Z. Lv, W. Yang, J. Phys. Chem. Solids 72 (2011) 773-778.

[11] T.F. Yi, J. Shu, Y.R. Zhu, X.D. Zhu, C.B. Yue, A.N. Zhou, R.S. Zhu, Electrochim. Acta54 (2009) 7464-7470.

[12] Y.H. Yin, S.Y. Li, Z.J. Fan, X.L. Ding, S.T. Yang, Mater. Chem. Phys. 130 (2011)186-190.

[13] Y. Wang, W. Zou, X.Y. Dai, L.D. Feng, H.Q. Zhang, A.J. Zhou, J.Z. Li, Ionics (2014), http://dx.doi.org/10.1007/s11581-014-1103-6.

[14] T. Yuan, R. Cai, Z. Shao, J. Phys. Chem. C 115 (2011) 4943-4952.

[15] L. Zhao, Y.S. Hu, H. Li, Z. Wang, L. Chen, Adv. Mater. 23 (2011) 1385-1388.

[16] H. Pan, L. Zhao, Y.S. Hu, H. Li, L. Chen, Chemsuschem 5 (2011) 526-529.

[17] H.Q. Zhang, Q.J. Deng, C.X. Mou, Z.L. Huang, Y. Wang, A.J. Zhou, J.Z. Li, J. Power Sources 239 (2013) 538-545.

Sources 239 (2013) 538e545.

[18] E. Matsui, Y. Abe, M. Senna, A. Guerfi, K. Zaghib, J. Am. Ceram. Soc. 91 (2008)1522-1527.

[19] J. Lim, E. Choi, V. Mathew, D. Kim, D. Ahn, J. Gim, S.H. Kang, J.

[20] Kim, J. Electrochem. Soc. 158 (2011) A275-A280. J.-G. Kim, D. Shi, M.-S. Park, G. Jeong, Y.-U. Heo, M. Seo, Y.-J. Kim, J.H. Kim,S.X. Dou, Nano Res. 6 (2013) 365-372.

[21] S. Huang, Z. Wen, J. Zhang, X. Yang, Electrochim. Acta 52 (2007) 3704-3708.

[22] S. Huang, Z. Wen, J. Zhang, Z. Gu, X. Xu, Solid State Ionics 177 (2006) 851-855.

[23] S. Huang, Z. Wen, X. Zhu, Z. Gu, Electrochem. Commun. 6 (2004) 1093-1097.

[24] C.C. Li, Q.H. Li, L.B. Chen, T.H. Wang, ACS Appl. Mater. Interfaces 4 (2012)1233-1238.

[25]M. Marinaro, F. Nobili, R. Tossici, R. Marassi, Electrochim. Acta 89 (2013) 555-560.

[26] S. Huang, Z. Wen, B. Lin, J. Han, X. Xu, J. Alloys Compd. 457 (2008) 400-403.

[27] J. Shu, L. Hou, R. Ma, M. Shui, L. Shao, D. Wang, Y. Ren, W. Zheng, RSC Adv. 2(2012) 10306-10309.

[28]X. Li, C. Lai, C. Xiao, X. Gao, Electrochim. Acta 56 (2011) 9152-9158.

[29] M.M. Rahman, J.Z. Wang, M.F. Hassan, D. Wexler, H.K. Liu, Adv. Energy Mater. 1 (2011) 212-220.

[30] Y.Q. Wang, L. Gu, Y.G. Guo, H. Li, X. He, S. Tsukimoto, Y. Ikuhara, L. Wan, J. Am.Chem. Soc. 134 (2012) 7874-7879.

[31] Y. Wang, A. Zhou, X. Dai, L. Feng, J. Li, J. Li, J. Power Sources 266 (2014) 114-120

[32] Prosini PP, Mancini R, Petrucci L, Contini V, Villano P., Solid State Ionics. 2001; 144(1):185.

[33] S. Y. Venyaminov and F. G. Prendergast, Analytical biochemistry 248 (1997) 234–245

[34] C.Lin, M.O. Lai, L.Lu, H. Zhou, Y.Xin, J. power sources 244(2013)272-279.

[35] M.M. Rahman, J.Z. Wang, M.F. Hassan, S. Chou, D. Wexler, H.K. Liu, , J. of Power Sources 195 (2010) 4297.

[36] J. Jamnik, J. Maier, Physical Chemistry Chemical Physics 5 (2003) 5215.

[37] X.Q. Yu, J.P. Sun, K. Tang, H. Li, X.J. Huang, L. Dupont, J. Maier, Physical Chemistry Chemical Physics11 (2009) 9497.

[38] C.-Y. Lin, J. G.Duh, J. Alloys and Compounds 509 (2011) 3682–3685

[39] H. Wu, S. Chang, X. Liu, L. Yu, G. Wang, D. Cao, Y. Zhang, B. Yang, P. She, Solid State Ionics (2013) 13-18.

[40] G.-Y. Liu, H.-Y. Wang, G.-Q. Liu, Z.-Z. Yang, B. Jin, Q.-C. Jiang, Electrochim. Acta 87(2013) 218-223.

[41] Emad M. Masoud, Alloys and compounds 651(2015)157-163.

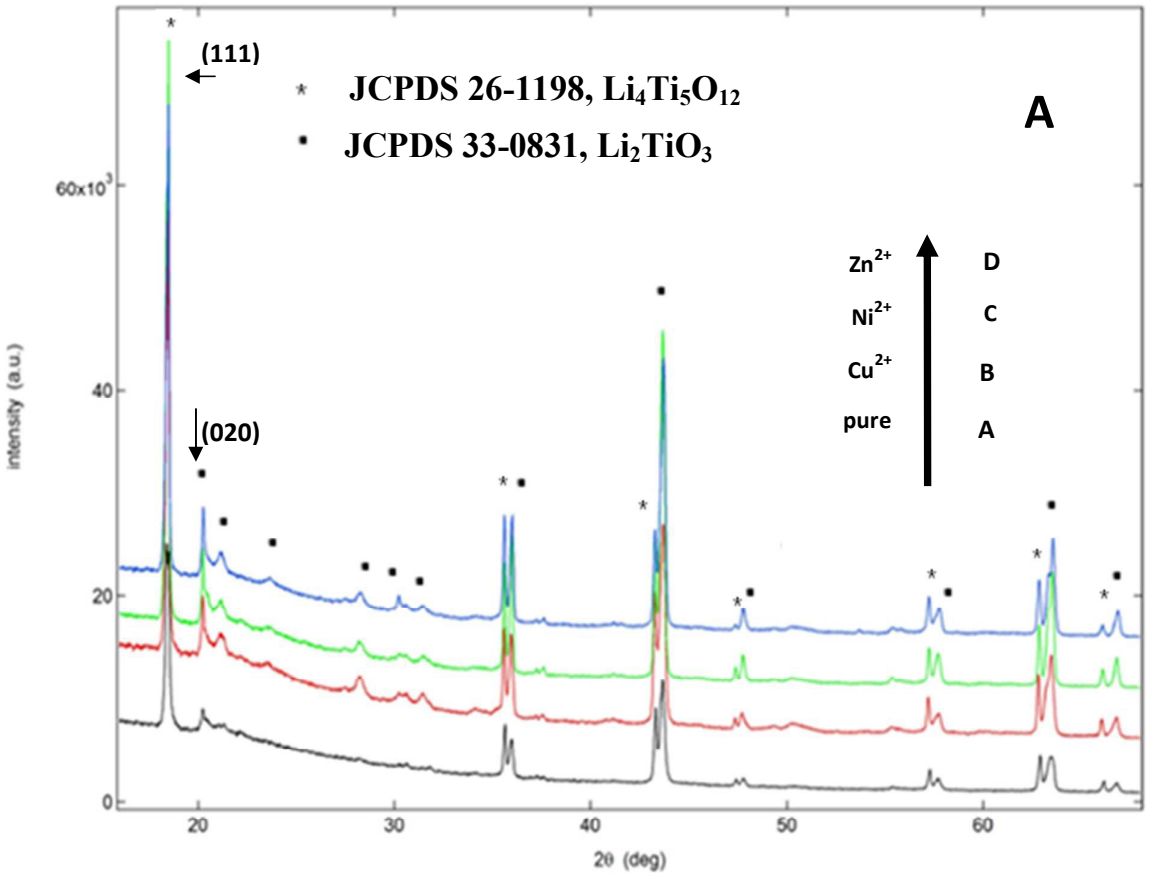

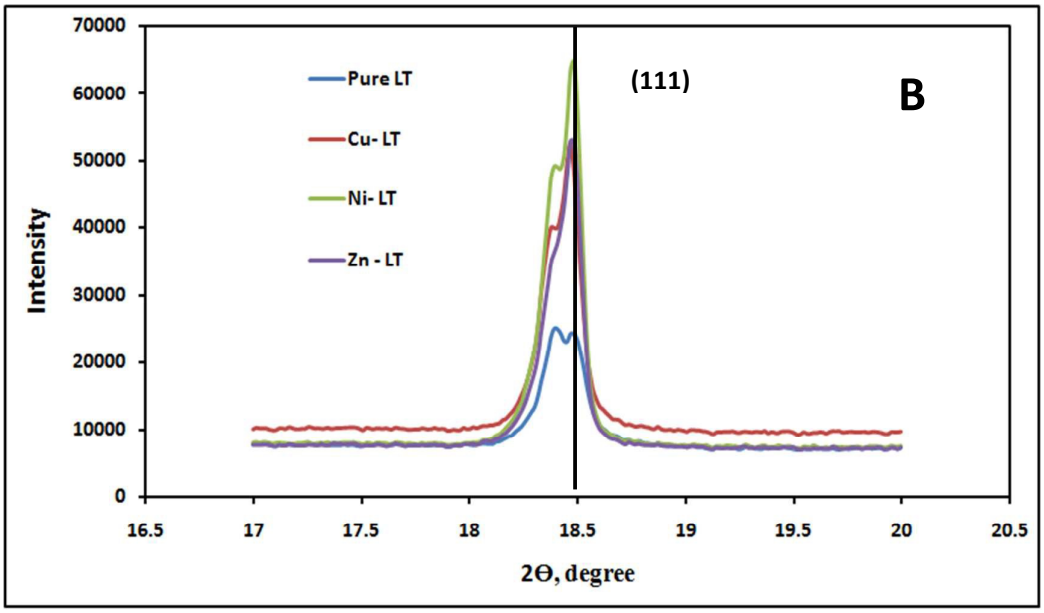

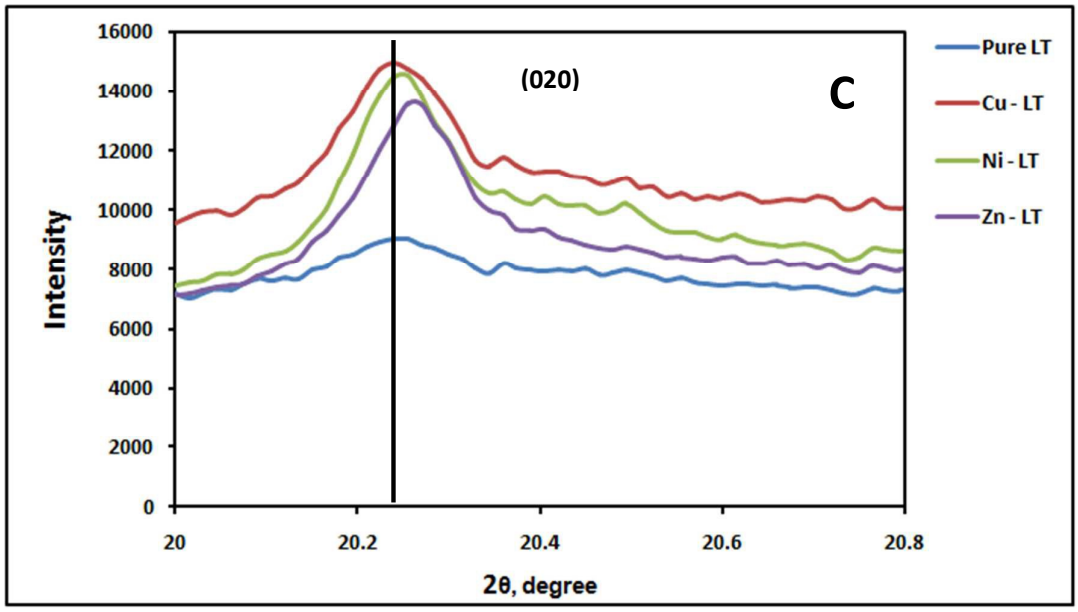

Fig. 1 X-ray diffraction patterns of A) pure and doped lithium titanates composites, B) partially enlarged drawing of $Li_4Ti_5O_{12}$ peak (111) and C) partially enlarged drawing of Li_2TiO_3 peak (020).

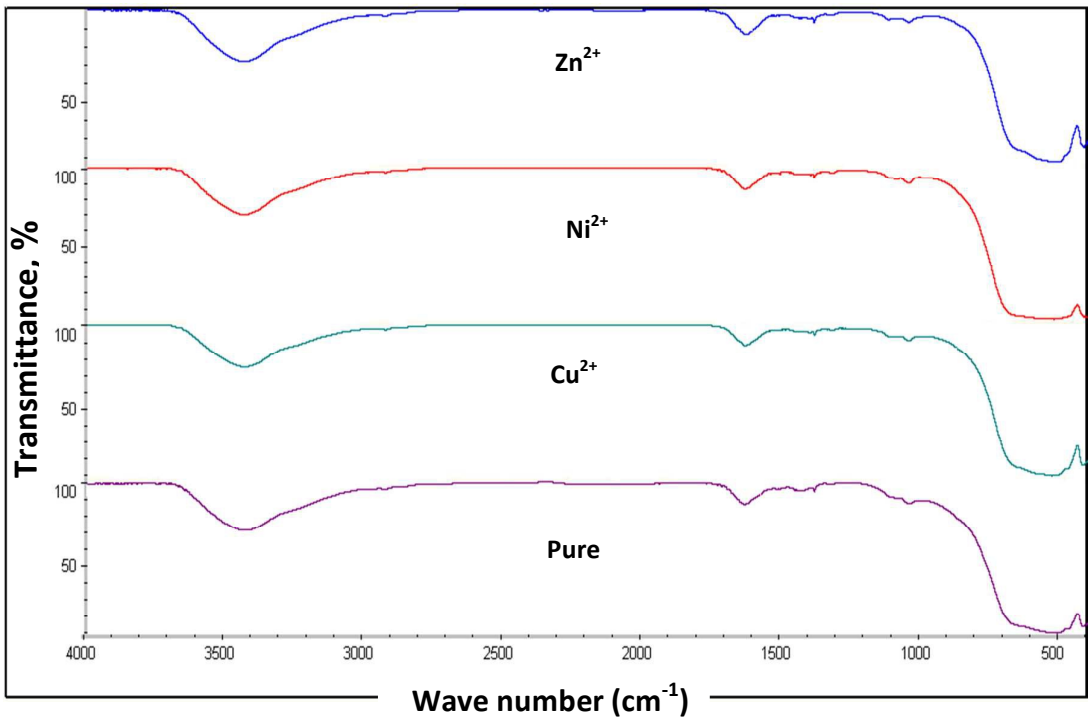

Fig.2 FT-IR patterns of pure and doped lithium titanates composites.

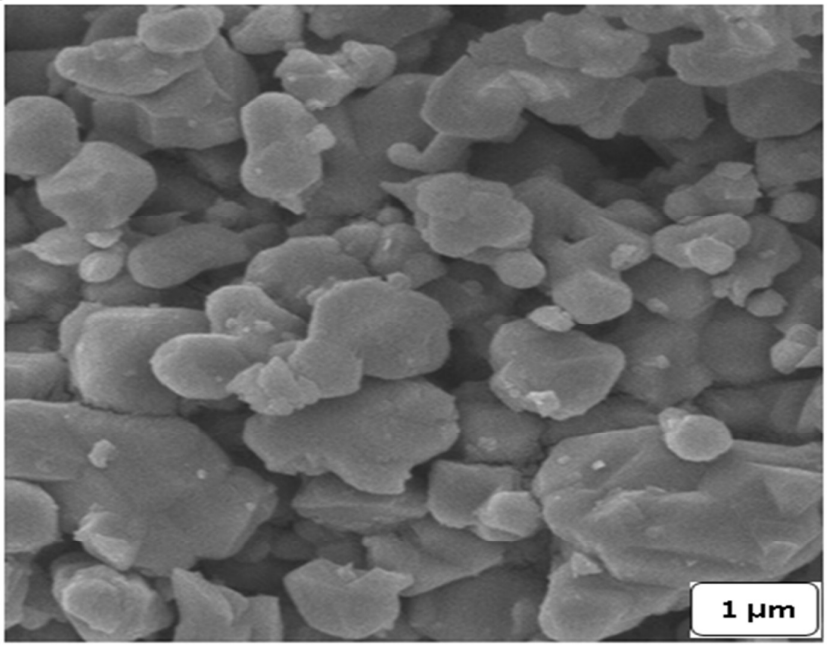

. **Fig.3 SEM of pure lithium titanates composite**

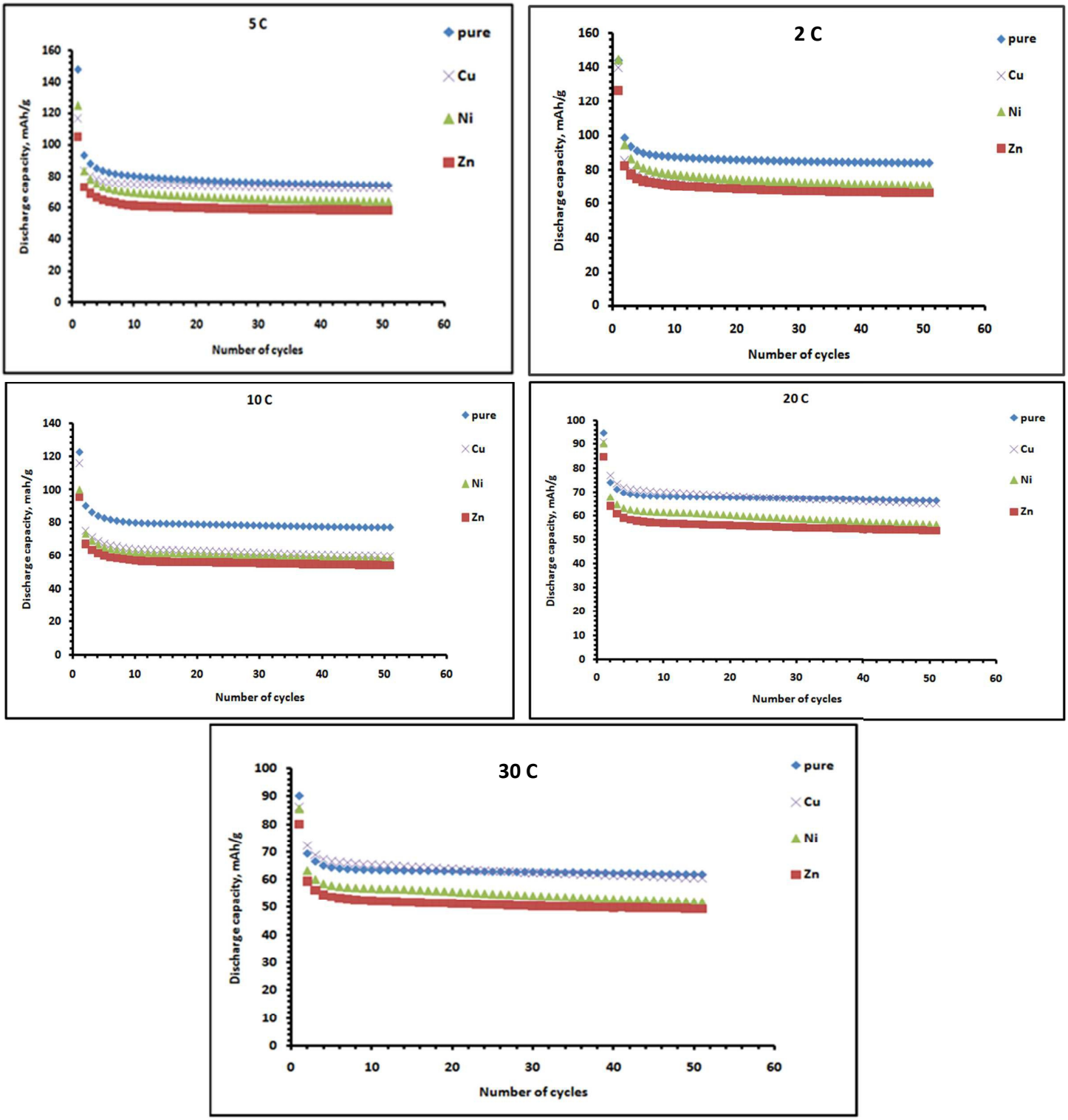

Fig.4 cycling performance of pure and doped lithium titanates composites at different rates (high rate).

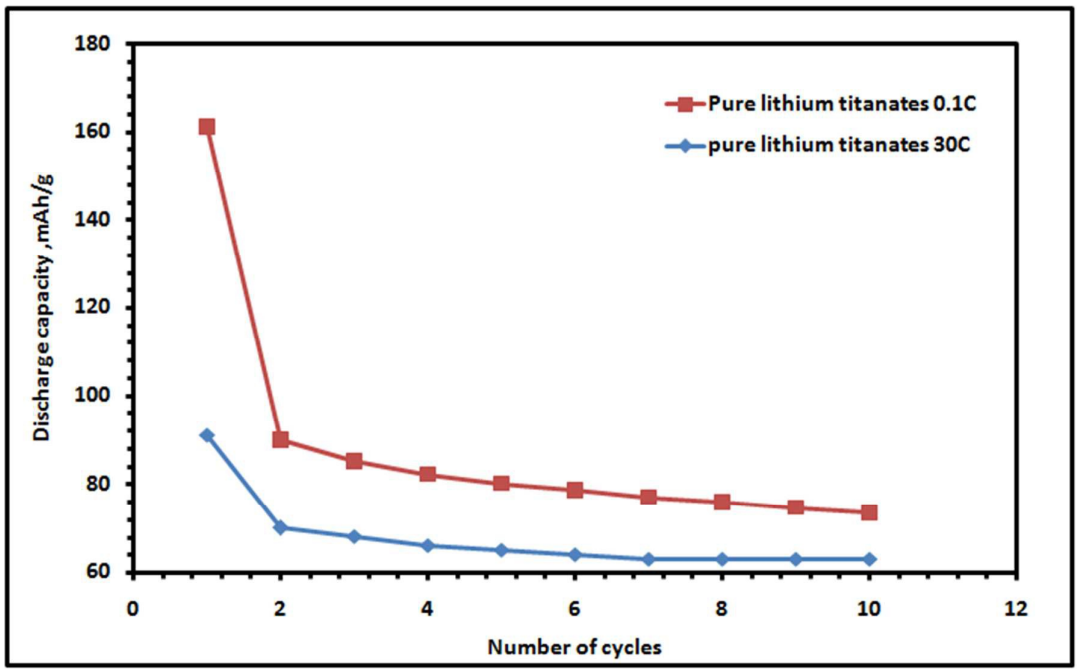

Fig. 5 cycling performance of pure lithium titanates composite at low (0.1C) and high (30C) rates.

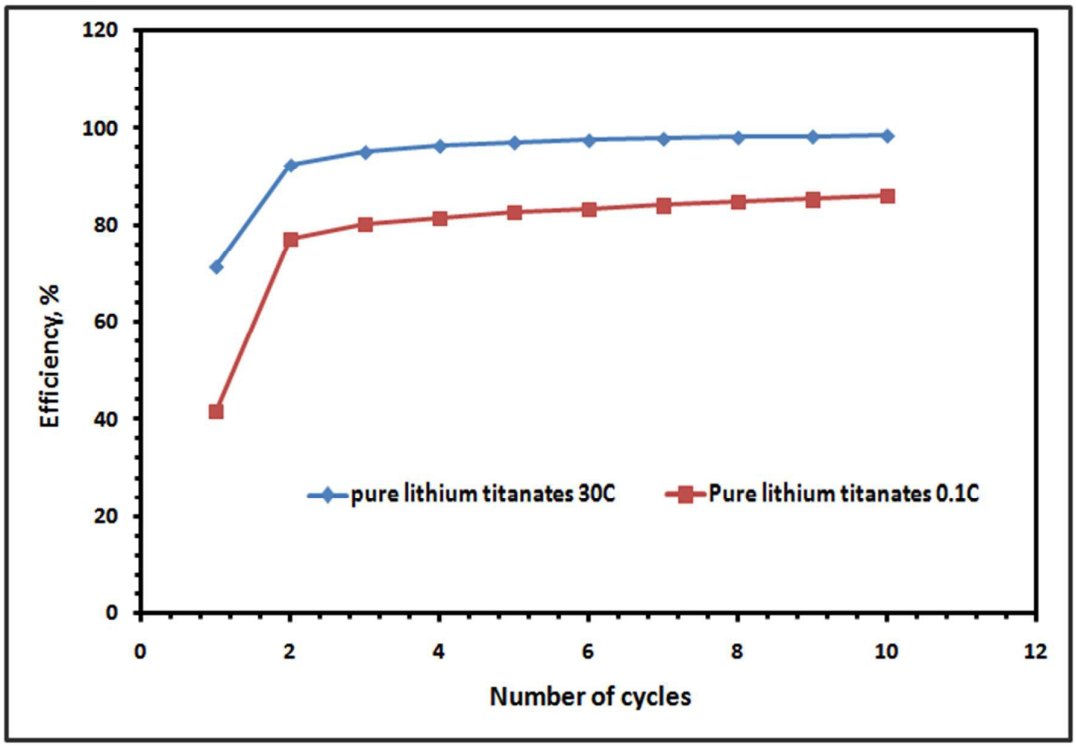

Fig. 6 Efficiency against cycle number for pure lithium titanates composite at low (0.1C) and high (30C) rates.

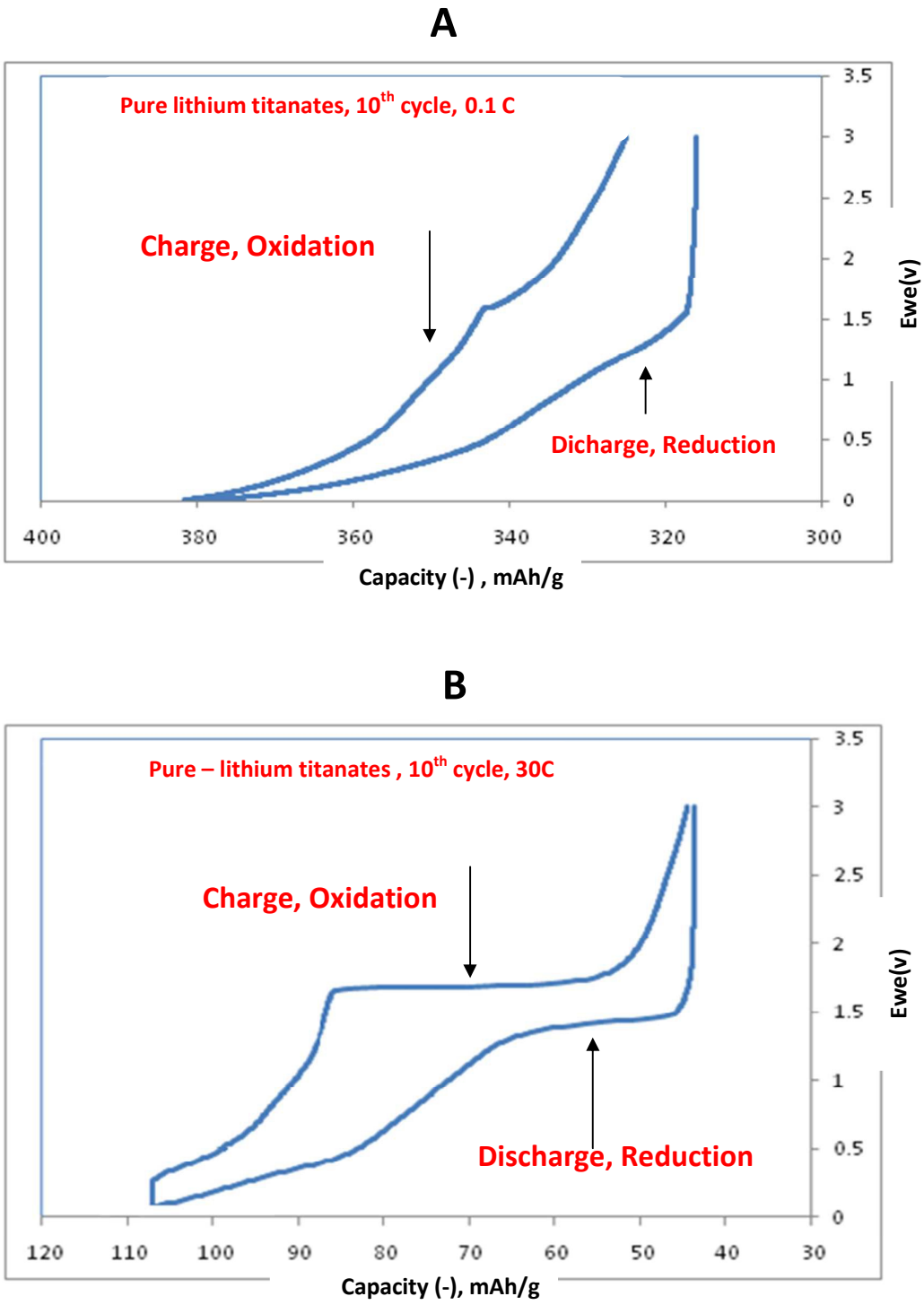

Fig. 7 Galvanostatic lithium insertion/ extraction curves for the 10th cycle of pure lithium titanates composite at low (0.1C) and high (30C) rates between 0-3V.

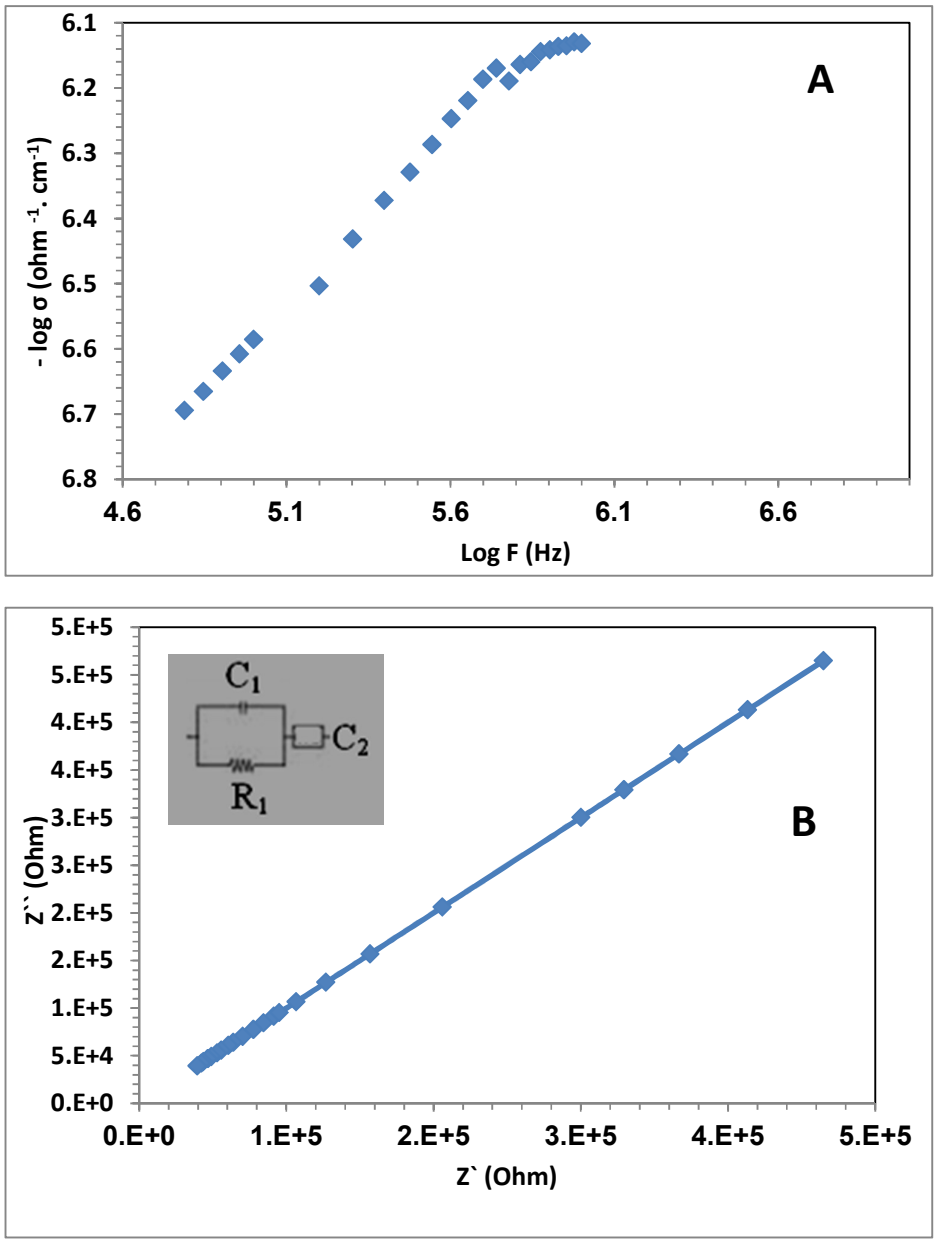

Fig. 8 AC- electrical conductivity properties; A) Frequency dependence of ionic conductivity and B) complex impedance for pure lithium titanates composite at room temperature (295 K).

Table1. Lattice parameter and unit cell volume of $Li_4Ti_5O_{12}$ phase, calculated from x-ray peak analysis (111), in all pure and doped lithium titanates (LT) composites .

Sample	a (Å)	Unit cell volume $(Å)^3$
LT- pure	0.8354	583.1
LT- Ni^{2+}	0.8363	584.2
LT-Cu^{2+}	0.8368	586.1
LT-Zn^{2+}	0.8369	586.2

Table2. Unit cell volume and weight ratio of Li_2TiO_3 phase, calculated from x-ray peak analysis (020), in all pure and doped lithium titanates (LT) composites

Sample	Unit cell volume $(Å)^3$	Weight ratio (%)
LT- pure	427.01	22.23
LT- Ni^{2+}	427.01	31.50
LT-Cu^{2+}	427.01	36.77
LT-Zn^{2+}	427.01	35.60

Table 3. Values of initial discharge capacity and Li-ion diffusion for pure and doped lithium titanates (LT) composites at low and high rates.

Sample	Initial discharge capacity ($mAhg^{-1}$)					Li-ion diffusion, $Dx10^{-13}$, cm^2s^{-1}
	0.1 C	**0.5 C**	**10 C**	**20 C**	**30 C**	
LT- pure	161	168	123	95	91	5.55
LT- Ni^{2+}	244	169	100	90	86	5.15
LT-Cu^{2+}	319	172	116	91	88	5.25
LT-Zn^{2+}	204	170	96	85	81	4.95

Table 4. Comparison of the electrochemical properties of pure lithium titanates composite ($Li_4Ti_5O_{12}/Li_2TiO_3$) at high rates.

Sample	Current density (C)	Potential range (V)	Initial capacity ($mAhg^{-1}$)	Capacity retention ($mAhg^{-1}$)	References
$Li_4Ti_5O_{12}$/ Li_2TiO_3(high content)	**30**	0 -3	91	65 After 50 cycles	This work
$Li_4Ti_5O_{12}$ /Li_2TiO_3 (very low content)	**10**	0-3	113	111 After 50 cycles	[31]
$Li_4Ti_5O_{12}$	**5**	0-3	33	31 After 10 cycles	[33]
$Li_4Ti_5O_{12}$	**30**	1-2.5	38	38 After 50 Cycles	[39]
$Li_4Ti_5O_{12}$	**20**	0.8 -2.5	62	37 After 50 cycle	[35]

Graphical Abstract

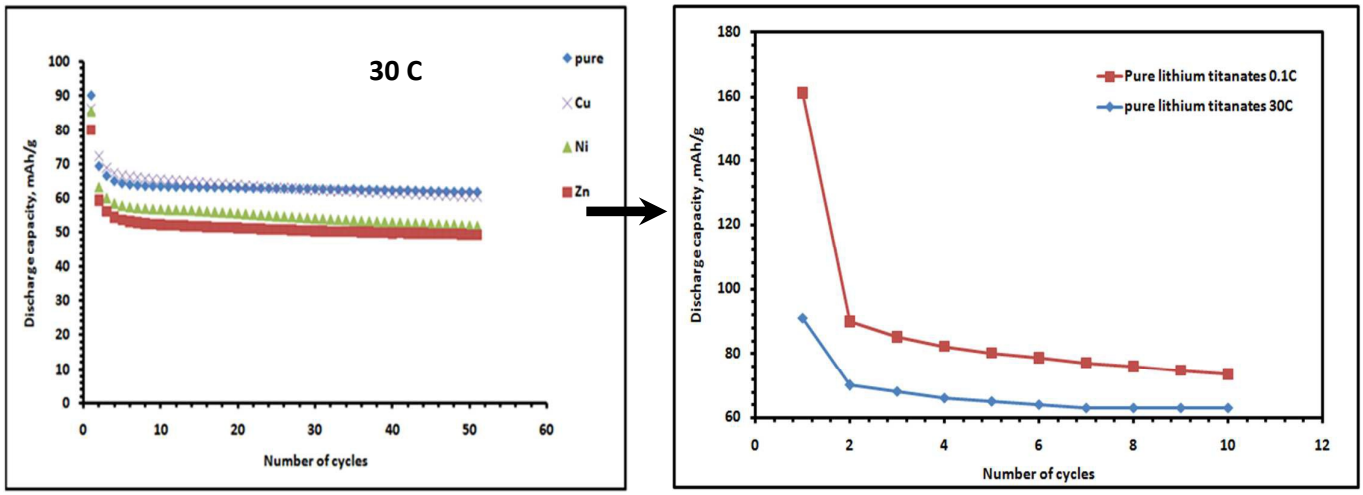

Pure lithium titanates composite sample is a promising anode for the high rate performance of lithium ion batteries